

August 1993

Amsterdam ITFA 93-18
UCSD/PTH 93-15

Non-gauge fixing approach to chiral gauge theories using staggered fermions

Wolfgang Bock^{1,#}, Jan Smit^{1,&} and Jeroen C. Vink^{2,*}

¹*Institute of Theoretical Physics, University of Amsterdam,
Valckenierstraat 65, 1018 XE Amsterdam, The Netherlands*

²*University of California, San Diego, Department of Physics,
9500 Gilman Drive 0319, La Jolla, CA 92093-0319, USA*

Abstract

We investigate a proposal for the construction of models with chiral fermions on the lattice using staggered fermions. In this approach the gauge invariance is broken by the coupling of the staggered fermions to the gauge fields. Motivated by previous results in the non-gauge invariant massive Yang-Mills theory and certain gauge-fermion models we aim at a dynamical restoration of the gauge invariance in the full quantum model. If the gauge symmetry breaking is not too severe, this procedure could lead in the continuum limit to the desired gauge invariant chiral gauge theory. This scenario is very attractive since it does not rely on gauge fixing. We investigate a simple realization of this approach in a U(1) axial-vector model with dynamical fermions in four dimensions.

e-mail: bock@phys.uva.nl

& e-mail: jsmit@phys.uva.nl

* e-mail: vink@yukawa.ucsd.edu

1 Introduction

An important unsolved problem in lattice field theory is the non-perturbative formulation of a chiral gauge theory on the lattice (for reviews see refs. [1, 2]). The naive lattice transcription of a quantum field theory involving fermions leads to unwanted fermion species, the so-called fermion doublers. Half of these couple with opposite chiral charge to the gauge fields, spoiling the chiral nature of the couplings, and the resulting theory in the scaling region is vector-like. To deal with these doublers, one has three options: I) Remove the fermion doublers by rendering them heavy, while keeping only one fermion in the physical spectrum [3-11], II) decouple them by turning off their interactions with the other particles [12] or III) use them as physical degrees of freedom [1, 13, 14].

When applied to chiral models, one has to reconcile the chosen regularization with gauge invariance. Many proposals are formulated such that local gauge invariance on the lattice is preserved [3,4,7-9,11]. For example, using a Wilson term to decouple the doublers, one introduces extra scalar fields to make this mass term gauge invariant. Alternatively one can sacrifice gauge invariance of the lattice model and transcribe the gauge fixed continuum action to the lattice [5, 6]. This avoids introducing extra scalar fields, but requires Fadeev-Popov and gauge fixing terms. It can be done with Wilson fermions as in refs. [5, 6], but also with staggered fermions. In either case one breaks the BRST symmetry, and one has to add counterterms to the action and tune their coefficients such that BRST invariance is restored in the continuum limit. This method is cumbersome from a technical point of view and in addition one has to worry about non-perturbative gauge fixing.

The method which we will focus on in this paper falls in class III. It relies on staggered fermions, which method uses the species doublers as Dirac-flavor components. The one-component staggered fermion fields do not carry explicit Dirac and flavor labels, these components are ‘spread out’ over the lattice. In the classical continuum limit this method leads to four flavors of Dirac fermions. It is possible to couple these Dirac flavors to the gauge fields such that the chiral target model is recovered in the classical continuum limit. We studied the method in ref. [15] for the case of a two-dimensional model with axial-vector couplings and concluded that it performed well for smooth external gauge fields. The important issue, however, is whether the same can be achieved also when the full quantum fluctuations are taken into account. The same method of coupling the staggered Dirac-flavor components has recently been successfully used for an investigation of a strongly coupled fermion-Higgs model [16].

In chiral gauge models we are confronted with the problem that the couplings of the staggered fermions to the gauge fields spoil the local gauge invariance. One possibility to overcome this difficulty is described in ref. [5], using the full machinery of gauge fixing. Alternatively one can attempt to avoid this and hope for a dynamical restoration of gauge invariance in the model without gauge fixing. By this we mean the following: carrying out the integration over all gauge field configurations in the path integral, the gauge degrees of freedom appear in the action as dynamical scalar fields with frozen radial mode; when these scalar fields decouple, gauge invariance is restored. As we shall see later there exist examples of non-chiral models where these scalar fields indeed decouple for suitable choices of the bare parameters. It is the subject of this paper to investigate this scenario for the staggered fermion approach to chiral gauge theories.

The outline of the paper is as follows: In sect. 2 we recall the scenario of dynamical gauge symmetry restoration and review the massive Yang-Mills model and a gauge-fermion model, as examples of models in which this scenario was found to work. In sect. 3 we define two staggered fermion models with axial-vector couplings to a $U(1)$ gauge field: the ISF

(invariant staggered fermion) model, which has a local gauge invariance and the NISF (non-invariant staggered fermion) model, which couples the staggered Dirac-flavor components in a way that allows for the construction of chiral models, but breaks local gauge invariance. The phase diagram of the ISF model will be presented in sect. 4. We shall also break the gauge symmetry of the ISF model by hand and argue that in this case the gauge invariance can again be restored dynamically. The phase diagram of the NISF model is presented in sect. 5 and from it we infer that the desired symmetry restoration does most probably not take place. We try to improve on this by modifying the model in sect. 6. Also here we find no evidence for the dynamical restoration of the gauge symmetry. Sect. 7 contains a summary of our results and gives an outlook to possible future investigations.

2 Restoration of gauge symmetry

There exist examples of gauge non-invariant lattice models where a dynamical restoration of gauge symmetry takes place. More precisely it has been found that one can add terms to a gauge invariant action that break the gauge symmetry, but provided the bare coupling constants of these terms are not too large, the low energy model remains the same. In our case the gauge symmetry is broken by the lattice regularization with staggered fermions, and there is no easy separation between a gauge invariant action and additional gauge symmetry breaking terms. The question arises if this symmetry breaking is sufficiently small that the chiral symmetry gets restored dynamically.

To explain the basic idea let us start first from a generic non-gauge invariant lattice action $S_{eff}(U')$. If also fermions are involved $S_{eff}(U')$ represents the effective action after integrating out the fermionic degrees of freedom in the path integral. The link field $U_{\mu x} = \exp(-iaA_{\mu x}) \in G$, with a the lattice distance, $A_{\mu x}$ the vector potential and G the compact gauge group. In the following we shall mostly use lattice units, $a = 1$. Assuming that the partition function is defined by the usual integration over the link field, it can be written as

$$\begin{aligned} Z &= \int DU' \exp S_{eff}(U') = \int DU \exp S_{eff}(\Omega_x U_{\mu x} \Omega_{x+\hat{\mu}}^\dagger) \\ &= \int DUDV \exp S_{eff}(V_x^\dagger U_{\mu x} V_{x+\hat{\mu}}) , \end{aligned} \quad (2.1)$$

where we have used in the second equation the gauge transformation $U'_{\mu x} = \Omega_x U_{\mu x} \Omega_{x+\hat{\mu}}^\dagger$ as a transformation of variables as well as the invariance of the Haar measure, $DU' = DU$. In the third equation we have added the trivial integration $1 = \int D\Omega$, and wrote $V_x = \Omega_x^\dagger$. In this way the gauge degrees of freedom Ω have been exhibited as an additional field in the path integral, which could be interpreted as a dynamical Higgs fields $V \in G$ with a frozen radial mode, $V_x^\dagger V_x = \mathbb{1}$. The new action $S_{eff}(V_x^\dagger U_{\mu x} V_{x+\hat{\mu}})$ is invariant under the local gauge transformations $U_{\mu x} \rightarrow \Omega_x U_{\mu x} \Omega_{x+\hat{\mu}}^\dagger$, $V_x \rightarrow \Omega_x V_x$.

The above manipulations turn any gauge non-invariant model into a related gauge invariant model, at the price of introducing an extra scalar field $V_x \in G$. The important question is if the resulting model still describes the physics of the underlying gauge invariant model, i.e. the models without adding the symmetry breaking terms to the action or, in our case, the model of the chirally invariant target model in the continuum. For instance, this requires that the V field decouples in the scaling region.

Before we turn to the question of dynamical gauge symmetry restoration in the staggered fermion model, let us first present two specific examples, namely the massive Yang-Mills theory and certain gauge-fermion models, which show that gauge non-invariant terms with

coefficients which are not too large, do not spoil gauge invariance after the integration over quantum fluctuations in the path integral has been carried out.

2.1 Massive Yang-Mills model

The massive $SU(2)$ Yang-Mills model is defined on the lattice by the euclidean action,

$$S_U = \frac{2}{g^2} \sum_{x\mu\nu} \text{Tr} U_{x\mu\nu} + \kappa \sum_{x\mu} \text{Tr} \{U_{\mu x} + U_{\mu x}^\dagger\} , \quad (2.2)$$

where g is the gauge coupling and κ the bare mass parameter in lattice units ($a = 1$). The $U_{x\mu\nu}$ denotes the usual plaquette variable on the lattice. The mass term in (2.2) breaks the local $SU(2)$ gauge invariance. After going through the steps of eq. (2.1) we find the action of the gauge invariant extension of the model,

$$S_{U,V} = \frac{2}{g^2} \sum_{x\mu\nu} \text{Tr} U_{x\mu\nu} + \kappa \sum_{x\mu} \text{Tr} \{V_x^\dagger U_{\mu x} V_{x+\hat{\mu}} + V_{x+\hat{\mu}}^\dagger U_{\mu x}^\dagger V_x\} , \quad (2.3)$$

which is the action of a gauged $SU(2) \times SU(2)$ non-linear sigma model. Note that the perturbative non-renormalizability of the model (2.2) causes no problems when the model is treated non-perturbatively.

The non-linear sigma model at $g = 0$ (i.e. for $U_{\mu x} = \mathbb{1}$) has a phase transition at $\kappa = \kappa_c(0) \approx 0.3$. For $g > 0$ this phase transition extends into the κ - g plane and separates a Higgs ($\kappa > \kappa_c(g)$) from a confinement phase ($\kappa < \kappa_c(g)$). We are interested here only in the scaling region at small bare gauge coupling g , where we find continuum behavior.

There are three scaling regions of interest: (A) When approaching the point $\kappa_c(0)$ from within the Higgs phase, we encounter the usual Higgs phenomenon. The spectrum contains the three massive gauge bosons and the Higgs particle. (B) When approaching the point $\kappa_c(0)$ from within the confinement phase we have a theory with confined scalar particles, much like QCD. (C) If we let g approach zero inside the confinement phase away from the Higgs-confinement phase transition $\kappa_c(g)$, the scalar particles acquire masses of the order of the cut-off and we recover the pure $SU(2)$ Yang-Mills system with only glueballs in the physical particle spectrum.

In case C there is a whole region in parameter space ($0 < \kappa < \kappa_c(g)$), where the physics in the scaling region is the same as at $\kappa = 0$, at which point the bare action is that of the gauge invariant Yang-Mills model. However, if we make the symmetry breaking too large (i.e. κ close to κ_c), the model changes and goes into a different phase in which the physics is no longer described by the pure Yang-Mills part of (2.2). It is also interesting to note in passing that in case (A) the gauge degrees of freedom V produce a genuine Higgs field, which acquires a non-frozen radial mode in the low energy action. The representation of the gauge group carried by this Higgs field is determined by the initial symmetry breaking.

2.2 Gauge-fermion models

As a second example we discuss restoration of gauge invariance in models with fermions in which the symmetry breaking resides in the fermionic part of the action. The model which we shall consider here, and in more detail in the next sections, has axial-vector couplings to $U(1)$ gauge fields,

$$S = - \int d^4x \sum_{f=1}^{N_F} \left\{ \bar{\psi}'_f \gamma_\mu (\partial_\mu + i q_f \gamma_5 A_\mu) \psi'_f + y \bar{\psi}'_f \psi'_f \right\} . \quad (2.4)$$

There are N_F fermion flavors with charges $q_f = \pm 1$, $f = 1, \dots, N_F$, such that the model is anomaly free. For $y = 0$ the action (2.4) is invariant under the local gauge transformation: $A_\mu(x) \rightarrow A_\mu(x) + \partial_\mu \omega(x)$, $\psi(x) \rightarrow (\Omega(x)P_L + \Omega^*(x)P_R)\psi(x)$, $\bar{\psi}(x) \rightarrow \bar{\psi}(x)(\Omega(x)P_L + \Omega^*(x)P_R)$, with $\Omega(x) = \exp i\omega(x)$ and $P_L = (1 - \gamma_5)/2$, $P_R = (1 + \gamma_5)/2$. A non-zero mass parameter y allows us to discuss the effect of gauge symmetry breaking by a fermion mass. We have put a prime on ψ and $\bar{\psi}$ to indicate the gauge in which the symmetry breaking has the simple mass term form $\sum_f y \bar{\psi}'_f \psi'_f$. Our target model is the gauge invariant model at $y = 0$. We shall show that this can be achieved even for nonzero y , provided it is not too large,

The lattice transcription of the action (2.4) with a single naive fermion field reads

$$S_{U,\psi'} = -\frac{1}{2} \sum_{x\mu} \left\{ \bar{\psi}'_x \gamma_\mu (U_{\mu x} P_L + U_{\mu x}^* P_R) \psi'_{x+\hat{\mu}} - \bar{\psi}'_{x+\hat{\mu}} \gamma_\mu (U_{\mu x}^* P_L + U_{\mu x} P_R) \psi'_x \right\} - y \sum_x \bar{\psi}'_x \psi'_x. \quad (2.5)$$

Because of the species doubling phenomenon this action reduces in the classical continuum limit to (2.4) with $N_F = 16$, where eight of the fermion species couple to the gauge fields with $q_f = +1$ and the remaining eight with $q_f = -1$. Note that with these charges the model is anomaly free and equivalent to QED with 16 flavors. The model we shall actually study numerically is a staggered fermion reduction of (2.5) in which the number of flavors is reduced by a factor of two (four q_f 's equal to $+1$ and four equal to -1). This model we shall call in the following the ISF model. However, in order not to overload the reader here with the details of the staggered fermion formalism, we shall continue for the moment with (2.5) as its properties are qualitatively the same as the ISF model.

For $y = 0$ the action (2.5) is invariant under the local gauge transformations,

$$U_{\mu x} \rightarrow \Omega_x U_{\mu x} \Omega_{x+\hat{\mu}}^*, \quad \psi'_x \rightarrow (\Omega_x P_L + \Omega_x^* P_R) \psi'_x, \quad \bar{\psi}'_x \rightarrow \bar{\psi}'_x (\Omega_x P_L + \Omega_x^* P_R). \quad (2.6)$$

For non-zero y the mass term in the action breaks gauge invariance. We shall argue however, that as in the case of the massive Yang-Mills model, the physics in the scaling region remains the same as with $y = 0$, provided y is not too large. Our arguments below are based on the knowledge of Wilson-Yukawa models accumulated in recent years [17].

Starting from the gauge non-invariant action (2.5) and after going through similar steps as in (2.1) we find,

$$S_{U,V,\psi'} = -\frac{1}{2} \sum_{x\mu} \left\{ \bar{\psi}'_x \gamma_\mu (V_x^* U_{\mu x} V_{x+\hat{\mu}} P_L + V_{x+\hat{\mu}}^* U_{\mu x}^* V_x P_R) \psi'_{x+\hat{\mu}} - \bar{\psi}'_{x+\hat{\mu}} \gamma_\mu (V_{x+\hat{\mu}}^* U_{\mu x}^* V_x P_L + V_x^* U_{\mu x} V_{x+\hat{\mu}} P_R) \psi'_x \right\} - y \sum_x \bar{\psi}'_x \psi'_x. \quad (2.7)$$

The fields ψ' and $\bar{\psi}'$ are now seen to be screened from the gauge fields by the V fields and therefore are neutral with respect to the $U(1)$ gauge transformations

$$U_{\mu x} \rightarrow \Omega_x U_{\mu x} \Omega_{x+\hat{\mu}}^*, \quad V_x \rightarrow \Omega_x V_x, \quad \psi'_x \rightarrow \psi'_x, \quad \bar{\psi}'_x \rightarrow \bar{\psi}'_x. \quad (2.8)$$

To see how the symmetry gets restored it is useful to make a transformation of variables to new fermionic fields

$$\psi'_x = (V_x^* P_L + V_x P_R) \psi_x, \quad \bar{\psi}'_x = \bar{\psi}_x (V_x^* P_L + V_x P_R), \quad (2.9)$$

which leaves the integration measure invariant, $D\bar{\psi}D\psi = D\bar{\psi}'D\psi'$. The new fields ψ and $\bar{\psi}$ carry a U(1) charge since they transform as

$$\psi_x \rightarrow (\Omega_x P_L + \Omega_x^* P_R) \psi_x, \quad \bar{\psi}_x \rightarrow \bar{\psi}_x (\Omega_x P_L + \Omega_x^* P_R). \quad (2.10)$$

After inserting (2.9) into (2.7) we obtain an equivalent form of the action in terms of the ψ and $\bar{\psi}$ fields

$$\begin{aligned} S_{U,V,\psi} = & -\frac{1}{2} \sum_{x\mu} \left\{ \bar{\psi}_x \gamma_\mu (U_{\mu x} P_L + U_{\mu x}^* P_R) \psi_{x+\hat{\mu}} - \bar{\psi}_{x+\hat{\mu}} \gamma_\mu (U_{\mu x}^* P_L + U_{\mu x} P_R) \psi_x \right\} \\ & -y \sum_x \bar{\psi}_x (V_x^2 P_L + V_x^{*2} P_R) \psi_x. \end{aligned} \quad (2.11)$$

The bare mass term in (2.5) has now turned into a Yukawa term with Yukawa coupling y . Since gauge invariance is broken in the model without V field, one may add a mass counterterm for the gauge bosons, which takes the form of a kinetic term for the radially frozen scalar field in the gauge invariant extension, cf. eq. (2.3) above,

$$S_{U,V} = \kappa \sum_\mu \left\{ V_x^* U_{\mu x} V_{x+\hat{\mu}} + V_{x+\hat{\mu}}^* U_{\mu x} V_x \right\}. \quad (2.12)$$

Models like (2.11) have been studied in the global symmetry limit with gauge interactions turned off, i. e. at $g = 0$ with $U_{\mu x} = 1$, where they reduce to pure Yukawa models. The phase diagram of the staggered fermion version (ISF) of the model is displayed in fig. 1. The full details of this model and its phase diagram will be explained in sects. 3 and 4. Beside the ferromagnetic (FM) and antiferromagnetic (AM) phases at large positive and negative κ there are two different symmetric phases in which the magnetization $v = \langle \sum_x V_x \rangle / \text{volume}$ vanishes. These two phases in fig. 1, PMW and PMS, are separated by a phase transition line $y_c(\kappa)$, of presumably second order. The phase diagram is invariant under a $\kappa \rightarrow -\kappa$ reflection which interchanges the FM and AM broken phases, cf. sect. 4. The details of the phase diagram depend on the charge of the scalar field in the Yukawa coupling: instead of the charge two field V^2 we could use for the discussion of the symmetry restoration also the charge one field V . A phase diagram for fermion-Higgs models where the $\kappa \rightarrow -\kappa$ symmetry is absent and the fermions couple to V instead of V^2 can be found in ref. [18]. There the two symmetric phases are separated by a funnel-like region containing a ferromagnetic phase. Such non-universal features are, however, not important for our purpose here.

At small $y < y_c(\kappa)$ the Yukawa model has three scaling regions: (A) One can approach the FM(W)-PMW phase transition from within the FM(W) phase. Then the spectrum contains massive fermions and in addition there is a Higgs particle and a massless Goldstone boson. (B) If one approaches the FM(W)-PMW phase transition from within the PMW phase the spectrum contains massless fermions, but also two light scalar particles associated with the V field. (C) Anywhere in the PMW phase, away from the phase boundaries, the scalar particles decouple and even though $y > 0$, the spectrum contains only free massless fermions. These properties agree qualitatively with treating the Yukawa coupling term in the action (2.11) as a perturbation. By interpreting $U_{\mu x}$ in (2.11) as an external gauge field, we draw the important conclusion that the fermions at small y are charged.

From the phase diagram of the Yukawa theory at small y we infer corresponding scaling regions (A-C) in the full theory with dynamical gauge fields, at small gauge coupling g . In (A) we have the Higgs phenomenon and massive fermions, in (B) we have electrodynamics with massless fermions and in addition massive charged scalars, while in (C) the scalars decouple. In the region (C) the desired gauge symmetry restoration takes place and we recover the target model: massless fermions interacting with the U(1) gauge fields.

For large y ($y > y_c(\kappa)$) we do not recover the physics of the target model. Previous investigations have shown that the effective action which describes the low energy physics in the PMS phase is more like eq. (2.7) and not like (2.11). The fermion spectrum contains only the ψ' fermions whose couplings to the bosonic particles vanish as a power of the lattice distance [17]. The ψ' fermions are neutral under the $U(1)$ gauge symmetry. They have masses, even in the PMS phase, which are generically of the order of the cut-off. Depending on details of the lattice model, the mass in the PMS phase can be tuned to zero (as in the Wilson-Yukawa models for a sufficiently large value of the Wilson-Yukawa coupling). In any case the scaling physics in the PMS phase is not that of the gauge invariant target model (2.4) at $y = 0$ because the fermions are neutral.

In section 4 we shall consider yet another way of breaking the gauge invariance in the lattice models, namely, by changing the normalization of γ_5 , making the replacement

$$\gamma_5 \rightarrow \kappa_A \gamma_5, \quad (2.13)$$

with $\kappa_A \neq 1$. This breaks gauge invariance on the lattice, which is compact $U(1)$, although in the classical continuum limit the model is still invariant under non-compact gauge transformations. Nevertheless, we shall show that in the quantum case there is a wide range of values of κ_A for which there is a PMW phase where symmetry restoration will take place.

Summarizing, our arguments for symmetry restoration in the chiral gauge-fermion models with staggered fermions depend crucially on the existence of a PMW phase in the global symmetry limit. This phase has the massless fermions of the classical target model, which interact gauge invariantly with the gauge field when it is switched on as an external field. In the interior of the PMW phase (region (C)) there are no scaling scalars. Hence, for dynamical gauge fields this may be considered as a satisfactory regularization of the target model.

Strictly speaking the models studied here numerically are not chiral since the charges q_f are chosen, for numerical reasons, such that the models are equivalent to vector models. However, the existence of a PMW phase depends presumably only on the relative smallness of the symmetry breaking and not on the chiral properties of the theory.

3 Staggered fermion models with axial-vector couplings

In this section we shall introduce lattice versions of the continuum model (2.4) which allows for a chiral set of charges q_f , using staggered fermions. This is most easily done in terms of 4×4 matrix fields $\Psi_x^{\alpha\kappa}$ and $\bar{\Psi}_x^{\kappa\alpha}$, where the indices α and κ act as Dirac and flavor indices, respectively [1]. Consider the following ansatz for a lattice action,

$$\begin{aligned} S_{U,\Psi'} = & -\frac{1}{2} \sum_{x\mu} \text{Tr} \left\{ \bar{\Psi}'_x \gamma_\mu (U_{\mu x}^{LL} P_L + U_{\mu x}^{RL} P_R) \Psi'_{x+\hat{\mu}} P_L - \bar{\Psi}'_{x+\hat{\mu}} \gamma_\mu (U_{\mu x}^{LL*} P_L + U_{\mu x}^{RL*} P_R) \Psi'_x P_L \right. \\ & \left. + \bar{\Psi}'_x \gamma_\mu (U_{\mu x}^{LR} P_L + U_{\mu x}^{RR} P_R) \Psi'_{x+\hat{\mu}} P_R - \bar{\Psi}'_{x+\hat{\mu}} \gamma_\mu (U_{\mu x}^{LR*} P_L + U_{\mu x}^{RR*} P_R) \Psi'_x P_R \right\} \\ & - y \sum_x \text{Tr} \left\{ \bar{\Psi}'_x \Psi'_x \right\}. \end{aligned} \quad (3.1)$$

The projectors $P_{L,R}$ on the left-(right-)hand side of Ψ' project on eigenstates of γ_5 in the Dirac (flavor) space. The $U_{\mu}^{LL}, \dots, U_{\mu}^{RR}$ may carry different representations of the gauge group. We restrict ourselves here to γ_5 as the only non-trivial flavor matrix.

As it stands, the action (3.1) has the same local gauge invariance as the $N_F = 4$ classical continuum model (2.4) if all components $\Psi_x^{\alpha\kappa}$ and $\bar{\Psi}_x^{\kappa\alpha}$ would be independent degrees of

freedom. However, such a model would have fermion doublers and would lead to a vector-like gauge model for all choices of U^{LL}, \dots, U^{RR} . The fermion doublers are situated at the boundary of the Brillouin zone in momentum space, i.e. near momenta $p_\mu = \pm\pi$. After restricting the momenta of the matrix fields such that

$$-\pi/2 < p_\mu \leq +\pi/2, \quad (3.2)$$

we loose the fermion doublers of the matrix field, but also gauge invariance. It is clear, however, that in the classical continuum limit, where the fields and their momenta go to zero (in lattice units), eq. (3.1) with the momentum restriction (3.2) goes over into the corresponding continuum model. Hence the full gauge invariance gets restored in this limit.

One might think that the cut-off in momentum space has to result in a non-local action. However, it is possible to express the action in a form that is local, using staggered fermion fields χ_x and $\bar{\chi}_x$. The connection with the $\Psi_x^{\alpha\kappa}$ and $\bar{\Psi}_x^{\kappa\alpha}$ is made by writing [1, 14]

$$\Psi_x = \frac{1}{8} \sum_b \gamma^{x+b} \chi_{x+b}, \quad \bar{\Psi}_x = \frac{1}{8} \sum_b (\gamma^{x+b})^\dagger \bar{\chi}_{x+b}, \quad (3.3)$$

where $\gamma^x \equiv \gamma_1^{x_1} \gamma_2^{x_2} \gamma_3^{x_3} \gamma_4^{x_4}$ and the sum extends over the 16 corners of a unit lattice hypercube, $b_\mu = 0, 1$. The substitution of (3.3) into the action (3.1) leads to a local action. In momentum space we have the relation [14]

$$\Psi_{\alpha\kappa}(p) = Z(p) \sum_b T_{\alpha\kappa,b}(p) \chi(p + \pi b), \quad -\pi/2 < p_\mu \leq +\pi/2, \quad (3.4)$$

where $T_{\alpha\kappa,b} = \sum_c \exp(ibc\pi) \gamma_{\alpha\kappa}^c / 8$ is a unitary matrix and $Z(p)$ is a non-vanishing function in the restricted momentum interval. This relation is derived in the appendix. It shows clearly that in the restricted momentum interval the Fourier components of the matrix field are independent.

By choosing appropriate link fields $U_\mu^{LL}, \dots, U_\mu^{RR}$, the fermions couple in different ways to the gauge field. For example, with

$$U_\mu^{LL} = U_\mu^{RL} = U_\mu^{LR} = U_\mu^{RR}, \quad (3.5)$$

the four fermions couple vector-like; with

$$U_\mu^{LL} = U_\mu^{LR} = U_\mu, \quad U_\mu^{RL} = U_\mu^{RR} = 1 \quad (3.6)$$

we have a left model in which only the four left-handed fermions couple to the gauge field; with

$$U_\mu^{LL} = U_\mu^{LR} = U_\mu, \quad U_\mu^{RL} = U_\mu^{RR} = U_\mu^* \quad (3.7)$$

we have a four fermion version of the axial-vector model (2.4) with all $q_f = +1$ and finally with

$$U_\mu^{LL} = U_\mu^{RR} = U_\mu, \quad U_\mu^{LR} = U_\mu^{RL} = U_\mu^* \quad (3.8)$$

we have the axial-vector model (2.4) with $q_{1,2} = +1$ and $q_{2,3} = -1$.

The key issue of gauge symmetry restoration can be investigated in model (3.1, 3.7). It is advantageous to choose this axial vector model, and not the left model (3.1, 3.6), because the staggered version of this model has a larger lattice symmetry group which reduces the number of counterterms in the scaling region. Generalizing $U_\mu \rightarrow U_\mu^q$ in (3.7) to actions with arbitrary integer charge q , it is straightforward to construct chiral anomaly free models by combining several actions (3.1, 3.7), e.g. $5(q = +1) + 4(q = -2) + 1(q = +3)$. For numerical

reasons we shall however study only the simple $1(q = +1) + 1(q = -1)$ anomaly free model, which is equivalent to a vector theory (eight flavor QED, for $y = 0$), obtained by adding mirror fermions (cf. sect. 4). Model (3.8) with an equal number of $+1$ and -1 axial charges can be easily modified such that it is exactly gauge invariant for $y = 0$ (see below). This gauge invariant version is the earlier mentioned ISF model which is a reduction of the naive fermion model in eq. (2.5) and which serves here as a reference model.

Similarly, one can construct staggered fermion models involving arbitrary coupling of the Dirac-flavor components of the staggered flavors to gauge or Higgs fields in a straightforward manner such that the target models are recovered in the classical continuum limit. We have shown that this works satisfactory in the two-dimensional U(1) version of the equal charge axial model [15]. For the Standard Model and Grand Unified Theories like SO(10) and SU(5) and the axial-vector model one can write down models in which the staggered fermion symmetry group is preserved [14]. This strategy of coupling the Dirac-flavor components of the staggered flavors has also recently been successfully applied to a fermion-Higgs model [16].

After the substitution (3.3) and working out the trace in (3.1) one obtains the action in terms of the staggered fermion fields. For the equal charge axial model (3.1, 3.7), we find

$$S_{U,\chi'} = -\frac{1}{2} \sum_{x\mu} \left[c_{\mu x} \frac{1}{16} \sum_b \eta_{\mu x+b} (\bar{\chi}'_{x+b} \chi'_{x+b+\hat{\mu}} - \bar{\chi}'_{x+b+\hat{\mu}} \chi'_{x+b}) \right. \\ \left. + i s_{\mu x} \frac{1}{16} \sum_{b+c=n} \eta_{5x+b} (\eta_{\mu x+c} \bar{\chi}'_{x+b} \chi'_{x+c+\hat{\mu}} - \eta_{\mu x+b} \bar{\chi}'_{x+b+\hat{\mu}} \chi'_{x+c}) \right] - y \sum_x \bar{\chi}'_x \chi'_x, \quad (3.9)$$

where

$$c_{\mu x} = \text{Re } U_{\mu x}, \quad s_{\mu x} = \text{Im } U_{\mu x}, \quad n = (1, 1, 1, 1). \quad (3.10)$$

The staggered sign factors $\eta_{\mu x}$ are defined as $\eta_{\mu x} = (-1)^{x_1+\dots+x_{\mu-1}}$. The factor $\eta_{5x} = -\eta_{4x} \eta_{3x+4} \eta_{2x+\hat{3}+4} \eta_{1x+\hat{2}+\hat{3}+4} = -(-1)^{x_1+x_3}$ represents the Dirac γ_5 . In the classical continuum limit this action describes $N_F = 4$ flavors of axially coupled Dirac fermions with $q_f = +1$, $f = 1, \dots, 4$.

For the axial model (3.1, 3.8) with $q_{1,2} = +1$ and $q_{3,4} = -1$, we find similarly,

$$S_{U,\chi'} = -\frac{1}{2} \sum_{x\mu} \left[c_{\mu x} \eta_{\mu x} (\bar{\chi}'_x \chi'_{x+\hat{\mu}} - \bar{\chi}'_{x+\hat{\mu}} \chi'_x) \right. \\ \left. + i s_{\mu x} \varepsilon_x \eta_{\mu x} (\bar{\chi}'_x \chi'_{x+\hat{\mu}} - \bar{\chi}'_{x+\hat{\mu}} \chi'_x) \right] - y \sum_x \bar{\chi}'_x \chi'_x. \quad (3.11)$$

The sign factor $\varepsilon_x = (-1)^{x_1+\dots+x_4}$ represents the product of the two γ_5 's in Dirac and flavor space. From the substitution (3.3) we would find hypercubical averages as in (3.9) above, but we have chosen to replace those according to $\frac{1}{16} \sum_b f_{x-b} \rightarrow f_x$. This leads to the same classical continuum limit and makes the model invariant under local gauge transformations (see below). The form (3.11) also follows by applying the familiar 'spin diagonalization' transformation [19] to the naive fermion action (2.5), which produces a sum of four actions equivalent to (3.11), and keeping only one of these.

In the equal charge axial model (3.9) the projection on eigenstates of the Dirac γ_5 leads to non-local couplings in the η_5 term of (3.9), which prevents the gauge invariance of the naive fermion model (3.1) to be carried over to its staggered fermion reduction. Hence we shall refer to this model as the non-invariant staggered fermion (NISF) model. In a similar fashion we would lose gauge invariance in the left model (3.1, 3.6) with staggered fermions.

In the model (3.1, 3.8) however, the projection involves an additional γ_5 in flavor space and the model is invariant under the local ‘ ε -symmetry’ of the staggered fermions: the action (3.11) with $y = 0$ is invariant under the local flavor non-singlet $U(1)$ transformation,

$$\chi'_x \rightarrow \exp(i\omega_x \varepsilon_x) \chi'_x, \quad \bar{\chi}'_x \rightarrow \bar{\chi}'_x \exp(i\omega_x \varepsilon_x), \quad U_{\mu x} \rightarrow \exp(-i\omega_x) U_{\mu x} \exp(i\omega_{x+\hat{\mu}}). \quad (3.12)$$

Therefore we shall call the model (3.11) in the following the invariant staggered fermion (ISF) model. As delineated in sect. 2, gauge symmetry is restored in this model also for $y > 0$, provided y is smaller than y_c . By making the transformation of variables, $\chi'_x = \exp(i\omega_x \varepsilon_x) \chi_x$, $\bar{\chi}'_x = \bar{\chi}_x \exp(i\omega_x \varepsilon_x)$ with $V = \exp i\omega_x$ we find the Yukawa form of the action in terms of the χ and $\bar{\chi}$ fields

$$S_{U,\chi} = -\frac{1}{2} \sum_{x\mu} \left[c_{\mu x} \eta_{\mu x} (\bar{\chi}_x \chi_{x+\hat{\mu}} - \bar{\chi}_{x+\hat{\mu}} \chi_x) + i s_{\mu x} \varepsilon_x \eta_{\mu x} (\bar{\chi}_x \chi_{x+\hat{\mu}} - \bar{\chi}_{x+\hat{\mu}} \chi_x) \right] - y \sum_x \left[\text{Re } V_x^2 + i \varepsilon_x \text{Im } V_x^2 \right] \bar{\chi}_x \chi_x, \quad (3.13)$$

with the $U(1)$ charge two scalar field V^2 . We remark that now, in contrast to the naive model, the fermion measure $D\bar{\chi}D\chi$ is not invariant under the transformations (3.12). The invariance of the measure is however recovered, after adding mirror fermion fields, which is required also for the use of the Hybrid Monte Carlo Algorithm (HMCA) in the numerical simulations, cf. sect. 4. So the final ISF model has four $q_f = +1$ and four $q_f = -1$.

In contrast to the ISF model the NISF model has lost its gauge invariance. The model can be thought of as being (almost) gauge invariant for the low momentum components of the gauge field while the symmetry violation increases for the high momentum components.

Following the procedure explained in the previous section, the gauge degrees of freedom in the non-invariant model can be interpreted as scalar fields and the action with those scalar fields is obtained by replacing the sine and cosine factor in (3.10) by

$$c_{\mu x} = \text{Re } V_x^* U_{\mu x} V_{x+\hat{\mu}}, \quad s_{\mu x} = \text{Im } V_x^* U_{\mu x} V_{x+\hat{\mu}}. \quad (3.14)$$

In our numerical work we shall furthermore restrict ourselves to the zero gauge coupling limit $U_\mu = 1$.

We have also introduced a further modification of the models that provides an additional parameter to monitor a possible restoration of gauge invariance. As can be seen in the staggered action (3.9), the γ_μ part of the target action leads only to a one-link coupling among the χ' and $\bar{\chi}'$ fields, whereas the $\gamma_\mu \gamma_5$ part involves three- and also five-link couplings. Therefore we expect that the $\gamma_\mu \gamma_5$ part of the action renormalizes differently from the γ_μ part and we may have to compensate for this with a finite renormalization factor in front of the $\gamma_\mu \gamma_5$ term. This leads to the replacement

$$s_{\mu x} \rightarrow \kappa_A s_{\mu x} \quad (3.15)$$

in the action (3.9). We can also modify the ISF model in this way. For $\kappa_A \neq 1$ the gauge invariance is broken and this model may be more similar to the NISF model.

For simplicity we use the same κ_A for the three and five link couplings. The appearance of both three and five link couplings in the $\gamma_\mu \gamma_5$ term, is an awkward feature of the action (3.9), because the three and five link terms may renormalize differently. Furthermore, a canonical construction of a transfer matrix requires that the couplings are confined within a hypercube. We can arrange for this, by replacing the five link terms in (3.9) by equivalent three link terms, which have the same classical continuum limit. We have sometimes used

such a modified form of the action instead of (3.9), but did not find a significant difference in the measured observables.

The crucial question now is whether the breaking of gauge invariance in the NISF model is sufficiently weak that we can have symmetry restoration in a PMW scaling region. The mechanism for this would be similar to that in the ISF model, for which the gauge degrees of freedom V_x can be explicitly transformed into a Yukawa term (cf. (3.13)), leading to charged massless fermions in the symmetric phase at weak Yukawa coupling. For the NISF model we cannot explicitly transform the V_x 's into a Yukawa coupling, but the same mechanism may take place effectively in the low momentum modes where the symmetry breaking is weak. The high momentum modes might primarily lead to a 'renormalization of γ_5 ', to be compensated by κ_A . We can get an idea of the sensitivity to a mismatch in κ_A values by studying the effect of $\kappa_A \neq 1$ in the ISF model. A major danger to the above mentioned scenario is that unlike the case of the massive Yang-Mills model and the ISF model, we cannot easily control the strength of the gauge symmetry breaking in the NISF model.

4 Phase diagram of the ISF model

To determine the phase structure of the ISF and NISF models we shall compute numerically the dependence of a number of local order parameters on the bare coupling parameters κ , y and κ_A . We use the Hybrid Monte Carlo method, which requires a positive definite fermion determinant. The fermion matrix for the ISF and NISF models can be obtained from the actions (3.11) and (3.9) by writing them in the form

$$S_{ISF} = -\overline{\chi} M_{ISF} \chi', \quad S_{NISF} = -\overline{\chi} M_{NISF} \chi'. \quad (4.1)$$

The fermion determinant, $\text{Det } M$, is not positive definite, but this we cure by replacing it by $\text{Det } (M^\dagger M)$ which is manifestly positive definite. This amounts to adding a mirror fermion field to the action, which couples to the matrix $M_{(N)ISF}^\dagger$. With this extra field both the ISF and the NISF model have equal number of fermions coupling with charge $q_f = +1$ and $q_f = -1$, which makes them vector-like and anomaly free.

We should mention here that the actions (3.11) and (3.9) for the ISF and NISF model are invariant under the discrete ε -symmetry

$$\chi'_x \rightarrow \varepsilon_x \chi'_x, \quad \overline{\chi}'_x \rightarrow \overline{\chi}'_x \varepsilon_x, \quad V_x \rightarrow \varepsilon_x V_x, \quad \kappa \rightarrow -\kappa, \quad (4.2)$$

which implies that the κ - y phase diagrams of the two models have to be invariant for $\kappa \rightarrow -\kappa$. Furthermore the actions are invariant under the symmetry

$$\chi'_x \rightarrow i\varepsilon_x \chi'_x, \quad \overline{\chi}'_x \rightarrow \overline{\chi}'_x i\varepsilon_x, \quad y \rightarrow -y, \quad (4.3)$$

which implies that the two phase diagrams are also symmetric around the $y = 0$ axis. It is therefore sufficient to restrict ourselves to the half plane $y > 0$.

The numerical simulations were carried out mainly on a 4^4 lattice. A few simulations were also performed on larger lattices (6^4 and 8^4). We used periodic boundary conditions for the scalar fields. For the fermion fields periodic boundary conditions were used in the spatial direction and antiperiodic boundary conditions in the time direction. We typically accumulated a statistics of 500-3000 HMCA trajectories at each point in the phase diagrams, depending on the autocorrelation time for the various observables. The step size in the HMCA was adjusted such that the acceptance rate was between 60 and 80%.

The local observables which we shall consider are:
the magnetization,

$$v = \left| \left\langle \frac{1}{V} \sum_x V_x |_{\text{rot}} \right\rangle \right| , \quad (4.4)$$

where V is the lattice volume and the subscript “rot” indicates that the standard rotation technique has been applied to account for the drift of the magnetization vector $(1/V) \sum_x V_x$ on a finite system [20];

the staggered magnetization,

$$v_{st} = \left| \left\langle \frac{1}{V} \sum_x \varepsilon_x V_x |_{\text{rot}} \right\rangle \right| ; \quad (4.5)$$

the energy associated with the kinetic term (2.12) for the scalar field,

$$E_\kappa = \left\langle \frac{1}{4V} \sum_{\mu x} \text{Re}(V_x^* V_{x+\hat{\mu}}) \right\rangle = \frac{1}{8V} \frac{\partial}{\partial \kappa} \ln Z , \quad (4.6)$$

with Z the partition function; and

the energy associated with the mass term for the fermions

$$E_y = \left\langle \frac{1}{V} \sum_x \chi'_x \bar{\chi}_x \right\rangle = \frac{1}{V} \frac{\partial}{\partial y} \ln Z . \quad (4.7)$$

It also proved to be useful to keep track of the number N_{CG} of Conjugate Gradient Algorithm iterations, needed for an inversion of the fermion matrix to a given accuracy. This quantity is large, if the fermion matrix has eigenvalues close to zero. The observables v and v_{st} are order parameters for ferromagnetism and antiferromagnetism and are non-zero in the FM and AM phases, respectively. From the κ -dependence of v and v_{st} we determined the position of FM-PM and PM-AM phase transitions shown in fig. 1. A zero fermion mass would be a clear signal of the PMW phase, but it would require larger lattices to measure this mass reliably. Instead we have read off the position of the PMW-PMS phase transition from the y -dependence of the energy E_y . The energies E_κ and E_y can be used to get information about the order of the phase transition.

We now discuss the numerical results for the ISF model in more detail. In fig. 2a we have plotted the energy E_y as a function of y for $\kappa = 0$ and several values of the γ_5 renormalization factor κ_A (cf. (3.15)). The open squares were obtained at $\kappa_A = 1$, in which case the model is equivalent to the Yukawa model (3.13). The energy E_y has its steepest slope at the PMW-PMS phase transition which for $\kappa_A = 1$ is close to $y = 1.4$. At this point the curvature changes also its sign. It appears that the phase transition is of second order, which we infer from the absence of a jump in E_y on larger lattices and the absence of a hysteresis effect in thermal cycles. The energy E_y is very small, but still non-zero in the PMW phase, increases at the PMW-PMS phase transition and is large in the PMS phase. The approximate fall off $\propto 1/y$ at large y can be understood from the eigenvalue distribution of the fermion matrix M_{ISF} : We can write $E_y = (1/V) \langle \text{Tr} M_{ISF}^{-1} \rangle = (1/V) \langle \sum 1/(\lambda(y) + y) \rangle$. The sum extends over all eigenvalues λ of the off-diagonal part of the fermion matrix M_{ISF} whose eigenvalue distribution turns out to be almost independent of y (see below).

The squares in fig. 2b show the y -dependence of N_{CG} . This quantity exhibits a maximum at the critical value of y indicating that the PMW-PMS phase transition is associated with the occurrence of small eigenvalues of the fermion matrix M_{ISF} . We will come back to this point at the end of this section.

As we mentioned in the previous sections, it is interesting to investigate the ISF model with different κ_A . Gauge invariance is broken for $\kappa_A \neq 1$ and we loose the equivalence of the models (3.11) and (3.13). In the figs. 2a and b we have also included the results for E_y and N_{CG} for several values of $\kappa_A \neq 1$. Interestingly it can be seen from the shape of the curves that a PMW-PMS phase transition emerges for all $\kappa_A > 0$. The position of the PMW-PMS phase transition shifts to smaller values of y when the value of κ_A is lowered as is obvious from the y -dependence of the points with the steepest slope in fig. 2a and of the maximum in fig. 2b.

In fig. 3 we have plotted the approximate position of the PMW-PMS phase transition, as determined from figs. 2a and b for $\kappa = 0$ into a κ_A - y phase diagram. The data points fall within error bars on a straight line through the origin with slope ≈ 0.77 . We encounter here another example of restoration of gauge invariance: The gauge symmetry is broken in the lattice action, but we expect that the PMW phase leads to the same scaling physics for all $\kappa_A > 0$. Only at $\kappa_A = 0$, where the $\gamma_\mu \gamma_5$ part disappears completely from the action (3.11), the curve for E_y in fig. 2 shows no indication for a change of curvature at small y and the PMS phase extends most probably down to $y = 0$.

Some additional insight about the phase structure is obtained from the eigenvalue spectra of the fermion matrix M_{ISF} . The eigenvalues were computed with the Lanczos algorithm. In fig. 4 we have plotted the eigenvalues of the off-diagonal part $M_{ISF}^{off} = M_{ISF} - y\mathbb{1}$ in the complex plane, for four independent scalar field configurations which were generated with the HMCA on a 4^4 lattice at $\kappa = 0$, $y = 0.5$ and $\kappa_A = 0.3$. We found empirically that the eigenvalue distributions obtained at other values of y , with κ_A and κ kept fixed, have almost identical shape. In particular they always cut the real axis at the same distance h from the origin, which is ≈ 0.37 for $\kappa_A = 0.3$.

The distribution of M_{ISF} for some non-zero value of y with κ_A kept fixed is then approximately obtained by shifting the distribution shown in fig. 4 by an amount y along the real axis. This explains the observed behavior of N_{CG} in fig. 2b. For $y < h$ the origin is situated within the hole and N_{CG} is small since there are no eigenvalues near the origin. It develops a peak when $y \rightarrow h$, because eigenvalues come close to origin and it decreases again when y is increased beyond h . We conclude that $y_c \approx h$, which is consistent with the value obtained from fig. 3.

The width h of the eigenvalue distribution increases for increasing κ_A . For $\kappa_A = 1$ we find the eigenvalues to be arranged along the boundary of a circle and at larger κ_A along the boundary of an ellipse with the principal axis on the real axis. At $\kappa_A = 0$ the fermion matrix is anti-hermitian and the eigenvalues fall exactly on the imaginary axis. This gives additional support for the absence of a phase transition in y at $\kappa_A = 0$.

As is illustrated with this discussion, the appearance of a PMW phase at small y is associated with a hole in the eigenvalue distribution, which gives rise to the concave y -dependence of E_y for $y < y_c$ and to the peak in the number of CG iterations at $y = y_c$. We shall also look for these features in the NISF model to establish if a PMW phase emerges there, in which the gauge symmetry breaking due to the high momentum scalar modes is restored.

5 Phase diagram of the NISF model

We have seen in the previous section that the existence of the symmetry restoring PMW phase of the ISF model is stable against large deviations of κ_A from its preferred value 1. This suggests that a fine tuning of κ_A in the NISF model may not be necessary and it should

suffice to choose κ_A sufficiently large such that the PMW phase becomes clearly visible. In this section we discuss the phase diagram of the NISF model, mostly at fixed $\kappa = 0$, but for various values of κ_A . (Preliminary results for $\kappa \neq 0$ were reported in the first reference in [15].)

In fig. 5 we have plotted the energy E_y obtained in a thermal cycle as a function of y for $\kappa_A = 1$. The behavior is quite different from the one observed for this quantity in the ISF model. The energy exhibits a jump at $y \approx 0.8$ and a clear hysteresis effect is observed in the thermal cycle, indicating the presence of a first order phase transition. A similar behavior is found for $\kappa_A \neq 1$ and the position of the first order phase transition in the κ_A - y phase diagram is shown in fig. 6. Note that the phase boundary does not go through the origin as in fig. 3 and that there is even a phase transition at $\kappa_A = 0$.

The properties of the NISF model in the weak coupling region are unusual and quite different from those in the PMW phase of the ISF model. From the behavior of the energy E_κ and the order parameters v and v_{st} we find that the system can go into one of the following different states when lowering the parameter y from the PMS phase across the first order phase transition:

FM : $v \neq 0$, $v_{st} = 0$ and $E_\kappa > 0$.

PM₊: $v = 0$, $v_{st} = 0$ and $E_\kappa > 0$.

PM₀: $v = 0$, $v_{st} = 0$ and $E_\kappa = 0$.

PM₋: $v = 0$, $v_{st} = 0$ and $E_\kappa < 0$.

AM : $v = 0$, $v_{st} \neq 0$ and $E_\kappa < 0$.

We shall therefore denote the weak coupling region in the following as a multi-state (MS) region. Also the number of CG inversions N_{CG} shows a qualitatively different behavior in the NISF model compared to the ISF model. The quantity N_{CG} grows when approaching the PMS-MS phase transition within the PMS phase, then jumps to a small value when crossing this transition and remains approximately constant within the MS region.

Fig. 7 shows the energy E_κ as a function of y at $\kappa = 0$ and $\kappa_A = 0$ for several thermal cycles started at $y = 1.0$ in the PMS phase. The jumps in E_κ show that the FM-PMS, PM₊-PMS, PM₋-PMS and AM-PMS are of first order. Also the PM₀-PMS phase transition is of first order since the energy E_y exhibits a jump for all these transitions. The appearance of five (meta) stable states in the PMW phase indicates that the inclusion of the fermions produces additional (local) minima in the effective action for the scalar field V_x . The $\kappa \rightarrow -\kappa$ symmetry (4.2) relates the PM_± states and the FM with the AM state. Even on very small lattice volumes the local minima appear to be separated by very high energy barriers in configuration space since we have never observed tunneling events between the various states of the MS region. The frequency distribution of the states which results after a repeated crossing of the PMS-MS transition indicate that system has a slight preference for the PM₀ phase.

In contrast to the PMW phase of the ISF model, the MS region in the NISF model persists for $0 < y \lesssim 0.7$ at $\kappa_A = 0$. This indicates that this region is different from the PMW phase in the ISF model. It is not excluded, however, that a new phase, which harbors gauge symmetry restoration, is still present for smaller values of y , hidden inside the MS region. After scanning the various states of the MS region in the y and κ_A directions ($0 \leq \kappa_A \leq 2$, $0.1 \leq y \leq y_c(\kappa_A)$) on an 8^4 lattice we did not find any indication for the emergence of another phase transition.

At $\kappa_A = 0$ the $\gamma_\mu \gamma_5$ term in the fermion action is absent, and the only difference between the NISF model and the ISF model is the hypercubical average over $\text{Re}(V_x^* V_{x+\hat{\mu}})$ in the one-link γ_μ part of the action. This implies that the phenomenon of the MS region and the first order phase transition is induced by this hypercubical average. It suggests to study also

a modified model with the replacement

$$\frac{1}{16} \sum_b \text{Re}(V_{x-b}^* V_{x-b+\hat{\mu}}) \rightarrow \text{Re}(V_x^* V_{x+\hat{\mu}}) \quad (5.1)$$

in the one-link term of the action (3.9). In the classical continuum limit this modified model leads to the same target model. The modification also makes the NISF model more similar to the ISF model.

6 Phase diagram of the modified NIFS model

From the behavior of the observables v , v_{st} and E_κ we obtain the phase diagram in the κ - y plane shown in fig. 8, which applies to the case $\kappa_A = 2$. In contrast to the phase diagram of the NISF model without the replacement (5.1), we find no MS region at small y . The phase diagram contains only the strong coupling phases FM(S), PMS and AM(S). The FM(S)-PMS and PMS-AM(S) phase transitions are most likely of first order (dashed line) for $y \lesssim 1.4$ and of second order (full line) for $y \gtrsim 1.4$. The gap in E_κ , v and v_{st} is seen to increase when y is lowered.

The κ - y phase diagram at smaller values of κ_A looks very similar to the one shown in fig. 8, except that the FM(S)-PMS and PMS-AM(S) phase transitions appear to change from first to second order at a smaller value of y . For $\kappa_A = 0$ it appears to be second order for all y . This indicates that the point where the FM(S)-PMS and PMS-AM(S) phase transitions change their order has a similar κ_A -dependence as the phase transition line in the ISF model shown in fig. 3.

The apparent absence of a phase transition to a PMW phase at small y can be illustrated from the y -dependence of E_y . In fig. 9 we have displayed the energy E_y as a function of y for two values of κ_A and $\kappa = 0$, on a 4^4 lattice. The curve at $\kappa_A = 0$ (open squares) is identical with the one shown already in fig. 2, for which the PMS phase extends down to $y = 0$. The maximum of the curve at $\kappa_A = 2$ (filled squares) is only shifted a little bit to larger y , which indicates that the $\gamma_\mu \gamma_5$ term needs a large prefactor κ_A to become important. If we try to fix this κ_A by matching the peaks in fig. 9 to those for the ISF model shown in fig. 2, we see that the curve at $\kappa_A = 2$ of fig. 9 may be compared with the curve at $\kappa_A = 0.3$ in fig. 2. This implies that a relative factor $\kappa_A \approx 7$ is needed to scale the $\gamma_\mu \gamma_5$ term in the modified NISF model to the same strength as in the ISF model. There is, however, no indication that the curvature $\partial^2 E_y / \partial y^2$ changes sign, as for the curve at $\kappa_A = 0.3$ in fig. 2. Instead the energy appears to vanish linearly when the value of y is reduced. This indicates that a phase transition does presumably also not emerge when the volume is increased. Also in the other observables we did not find a sign for a phase transition at non-zero y .

These results show that by the replacement (5.1) we have managed to remove the MS region, but unfortunately we are now left with a phase diagram with only strong coupling phases.

According to the discussion at the end of sect. 3, the symmetry restoration and the appearance of a PMW phase is expected to depend crucially on the dynamics of the low momentum modes. The small 4^4 lattice, however, can only accommodate a few low momentum modes. To improve on this, we have included at $\kappa_A = 2$ also some results on a 6^4 lattice. All data points lie systematically slightly below the results on the 4^4 lattice, but also in this case there is no indication for a sign change in the curvature at small y which would reveal the emergence of the PMW phase. A simulation at larger values of κ_A was not possible with our resources of computer time since the number of CG iterations increases when κ_A is raised

and at the same time the statistics has to be increased to account for larger autocorrelation times.

Another possibility to enhance the low momentum modes of the scalar field, is to increase the value of κ towards a second order phase transition. So far we have considered $\kappa = 0$ where the scalar field correlation length is presumably of order one. Therefore the high momentum components in V_x are very abundant and might prevent restoration of gauge invariance. It is therefore important to study the phase structure in a region where the scalar field correlation length is larger. In the pure scalar U(1) model the correlation length of the scalar particles in the PMW diverges when $\kappa \nearrow \kappa_c^{FM-PM}$. Also in our model we could hope that by choosing κ sufficiently close to κ_c , we can increase the scalar field correlation length enough that a PMW phase opens up. As delineated above the FM(S)-PMS phase transition at small y is however of first order. This implies that the correlation length of the scalar particles stays bounded and our runs at larger κ show indeed no qualitative differences from the results for $\kappa = 0$. This is illustrated by the κ -dependence of E_y . Interestingly we find that E_y does not depend on κ for a given value of y and $\kappa < \kappa_c^{FM-PM}$. In fig. 10 we have monitored the κ -dependence of E_y for three representative values of y . This shows that a y -dependence of E_y as shown in fig. 9 for $\kappa = 0$ will also hold for other κ -values in the PMW phase. A simulation very close to the FM-PM phase at small y and a precise determination of the position of the first order transition is hindered by large hysteresis effects. Therefore we cannot exclude the possibility that on a much larger lattice the correlation length very close to κ_c increases enough to allow for the appearance of the desired PMW phase.

Additional evidence for the scenario that there is no PMW phase emerging for $\kappa \nearrow \kappa_c$ is obtained from the eigenvalue distributions of the fermion matrix M_{NISF} , modified here by the substitution (5.1). Fig. 11 contains the spectra of $M_{NISF}^{off} = M_{NISF} - y\mathbb{1}$ for four independent scalar field configurations, generated with the HMCA at the point $(\kappa, y, \kappa_A) = (0, 0.5, 2)$. The M_{NISF}^{off} spectra obtained at other values of y and κ , $\kappa_c^{PM-AM} < \kappa < \kappa_c^{FM-PM}$ with $\kappa_A = 2$ kept fixed, look similar, except that for $y \lesssim 0.5$ the width of the distribution on the real axis vanishes approximately proportionally to y . Fig. 11 suggests no formation of a hole inside the distribution which, as we explained in sect. 6, would be an indication for the emergence of a PMW phase with restoration of the gauge symmetry at small y .

7 Final remarks

We have started our discussion with examples where restoration of gauge invariance takes place, the massive Yang-Mills theory and gauge-fermion models, provided that the symmetry breaking due to the bare mass term is not too large. If the mass parameters are raised beyond a critical value the system is driven to another phase with scaling physics differing substantially from that of the original gauge invariant target model without mass terms. We aimed for a similar dynamical gauge symmetry restoration in our chiral staggered fermion models, in which the gauge symmetry is broken by the high momentum modes. A strong motivation for this approach is that it should work without recourse to gauge fixing.

In our approach gauge invariance is restored in the bare action by integrating over all gauge degrees of freedom (the ‘longitudinal components’), which emerge as dynamical scalar fields in our lattice action, and which we want to decouple. We have applied this approach to a U(1) model with axial-vector couplings, and tested it in two staggered fermion realizations, denoted as the NISF models.

The aim was to find in the reduction to external gauge fields, but keeping the scalars dynamical, a PMW phase (weak coupling symmetric phase), with massless charged fermions

coupled gauge invariantly to the gauge field, and scalars with masses of the order of the cut-off. Our numerical results indicate, however, no PMW phase in either NISF model. In the first NISF model we could only find a PMS phase (strong coupling symmetric phase) connected to large values of the bare coupling parameter y , and a multi-state region at small y where the desired gauge symmetry restoration presumably does not take place. In the second (‘modified’) NISF model our results suggest that the PMS phase extends down to $y = 0$. One reason for this negative result in the modified NISF model appears to be the unfortunate fact that the symmetric phase at small y is separated from the broken phase by a first order phase transition. Therefore the scalar field correlation length remains small in the entire symmetric phase and the symmetry breaking due to the high momentum scalar modes remains too large.

Nevertheless, we cannot completely exclude from our numerical results the possibility that at large values of κ_A , the renormalization factor of γ_5 , a PMW phase with the desired symmetry restoration could still emerge in the near vicinity of the FM-PM phase transition. This may require much larger lattices in order to allow for sufficient dominance of the low momentum modes in the scaling region. It is also possible that after adding different counterterms to the action the first order phase transition between the FM and PM phase at small y may be changed into a second order one. One could think here of higher derivative couplings for the scalar field, which suppress the high momentum modes. A frustrating fact is, however, that in practice our simple models fail because of the rapid increase of computational requirements with volume and with increasing κ_A .

A way out could be the following. To make gauge symmetry restoration work we need good control over the strength of the symmetry breaking, which was lacking in our simple models. A natural way to gain control would be to reduce the scalar field fluctuations on the scale of the fermionic lattice spacing. We could for instance use two lattices with spacings, a' for the fermions and a for the bosons, with $a' \ll a$. The bosonic field values on the a' lattice are obtained from the a lattice by interpolation, such that the minimum wavelength bosonic mode is relatively smooth on the scale of a' . The ratio a'/a would then be an important parameter controlling the strength of gauge symmetry breaking. In the limit $a'/a \rightarrow 0$ this would mean treating the fermions in the continuum (called ‘the desperate method’ in ref. [1]). The detailed implementation, however, of such a program is not so easy (cf. ref. [21] for work on interpolating lattice gauge fields).

As an alternative one could start from a gauge fixed continuum model and regularize it using the lattice and staggered fermions. The model then becomes very similar to the Rome proposal [5], which uses Wilson fermions. A non-perturbative test of this gauge fixing approach is difficult because of technical obstacles. One can still carry out simpler tests, like quenched simulations in gauge-fixed background configurations. Recently we have presented results in this direction for the case of a U(1) model with axial-vector couplings in two dimensions [15].

Acknowledgements

The numerical calculations were performed on the CRAY Y-MP4/464 at SARA, Amsterdam. This research was supported by the “Stichting voor Fundamenteel Onderzoek der Materie (FOM)”, by the “Stichting Nationale Computer Faciliteiten (NCF)” and by the DOE under contract DE-FG03-91ER40546.

Appendix

In this appendix we give the derivation of the momentum space relation (3.4). The formula is obtained by inserting

$$\chi_x = \frac{1}{V} \sum_q \sum_b \exp[i(q + b\pi)x] \chi_{q+b\pi} \quad (\text{A.1})$$

in the Frouier transform of eq. (3.3),

$$\Psi(p) = \frac{1}{8} \sum_c \sum_x \exp(-ipx) \gamma^{x+c} \chi_{x+c} . \quad (\text{A.2})$$

The χ_p in (A.1) is the Fourier transform of χ_x with momentum $p = q + b\pi$. The \sum_q in eq. (A.1) is the sum over the restricted Brillouin zone, $-\pi/2 < q_\mu \leq +\pi/2$. After writing $x = y + d$, with y on a lattice with double lattice distance, and d running over a hyper cube, we obtain,

$$\Psi(p) = \frac{1}{8V} \sum_q \sum_y \sum_{bcd} \exp[-i(p-q)y] \exp[-i(p-q)d + iqc + ib(c+d)\pi] \gamma^{c+d} \chi_{q+b\pi} , \quad (\text{A.3})$$

where we have used $\gamma^y = 1$ and $\exp(ipby) = 1$. Next we note that $\sum_y \exp[i(p-q)y] = \frac{V}{16} \delta_{p,q}$ for p, q in the restricted Brillouin zone, and use

$$\begin{aligned} \sum_d \exp[i(d+c)b\pi] \gamma_{\alpha\kappa}^{d+c} &= \sum_d \exp(idb\pi) \gamma_{\alpha\kappa}^d \\ &\equiv 8T_{\alpha\kappa, b} , \end{aligned} \quad (\text{A.4})$$

to obtain (3.4) with

$$Z(p) = \prod_\mu \exp(ip_\mu/2) \cos(p_\mu/2) \quad (\text{A.5})$$

(Note that in ref. [14] a factor 1/2 is missing in the expressions for T and $Z(p)$). By using the formula for irreducible representations of a group

$$\sum_g \mathcal{D}_{\alpha\kappa}^r(g) \mathcal{D}_{\beta\lambda}^s(g)^* = \frac{1}{\text{Tr } \mathcal{D}} \delta_{rs} \delta_{\alpha\beta} \delta_{\kappa\lambda} \quad (\text{A.6})$$

with a normalized sum, $\sum_g = 1$, for the case of the fundamental representation of the group of 32 elements $\pm\gamma^d$, and

$$\sum_b \exp[ib(c-d)\pi] = 16\delta_{c,d} , \quad (\text{A.7})$$

it is straightforward to check the unitarity of T .

References

- [1] J. Smit, Nucl. Phys. B (Proc. Suppl.) 4 (1988) 451.
- [2] M.F.L. Golterman, Nucl. Phys. B (Proc. Suppl.) 20 (1991) 528;
I. Montvay, Nucl. Phys. B (Proc. Suppl.) 26 (1992) 57;
D.N. Petcher, Nucl. Phys. B (Proc. Suppl.) 30 (1993) 50.

- [3] J. Smit, *Acta Physica Polonica* B17 (1986) 531 (Zakopane 1985);
L.H. Karsten, in *Field Theoretical Methods in Particle Physics*, ed. W. Rühl, Plenum (1980) (Kaiserslautern 1979);
J. Smit, *Nucl. Phys.* B175 (1980) 307;
P.D.V. Swift, *Phys. Lett.* B145 (1984) 256.
- [4] E. Eichten and J. Preskill, *Nucl. Phys.* B268 (1986) 179.
- [5] A. Borrelli, L. Maiani, G.C. Rossi, R. Sisto and M. Testa, *Phys. Lett.* B221 (1989) 360;
Nucl. Phys. B333 (1990) 355;
M. Testa, *Nucl. Phys. Proc. B (Proc. Suppl.)* 26 (1992) 228;
L. Maiani, *Nucl. Phys. B (Proc. Suppl.)* 29B,C (1992) 19;
G.C. Rossi, R. Sarno and R. Sisto, *Nucl. Phys.* B398 (1993) 101.
- [6] G.T. Bodvin and E.V. Kovacs, *Nucl. Phys. B (Proc. Suppl.)* 20 (1991) 546; *Nucl. Phys. B (Proc. Suppl.)* 30 (1993) 617.
- [7] S.V. Zenkin, *Phys. Lett.* B298 (1993) 159; *Nucl. Phys. B (Proc. Suppl.)* 30 (1993) 613.
- [8] D.B. Kaplan, *Phys. Lett.* B288 (1992) 342; *Nucl. Phys. B (Proc. Suppl.)* 30 (1993) 597.
- [9] C. Pryor, *Phys. Rev.* D43 (1991) 2669.
- [10] S.A. Frolov and A.A. Slavnov, *Phys. Lett.* B309 (1993) 344.
- [11] R. Narayanan and H. Neuberger, *Phys. Lett.* B302 (1993) 62.
- [12] J.L. Alonso, P. Boucaud, J.L. Cortes and E. Rivas, *Phys. Lett.* B201 (1988) 340; *Phys. Rev.* D40 (1989) 4123; *Phys. Lett.* B237 (1990) 476; *Phys. Rev.* D44 (1991) 3258;
J.L. Alonso, P. Boucaud, J.L. Cortes, F. Lesmes and E. Rivas, preprint DFTUZ-92-8 (hep-lat/9206005); *Nucl. Phys. B (Proc. Suppl.)* 29B,C (1992) 171.
- [13] J. Smit, *Nucl. Phys. B (Proc. Suppl.)* 26 (1992) 480.
- [14] J. Smit, *Nucl. Phys. B (Proc. Suppl.)* 29B,C (1992) 83.
- [15] W. Bock, J. Smit and J.C. Vink, *Nucl. Phys. B (Proc. Suppl.)* 605; preprint ITFA 93-13, UCSD/PTH 93-13 (hep-lat/9306012).
- [16] W. Bock, J. Smit and J.C. Vink, *Phys. Lett.* B291 (1992) 297;
W. Bock, C. Frick, J. Smit and J.C. Vink, *Nucl. Phys.* B400 (1993) 309; *Nucl. Phys. B (Proc. Suppl.)* 30 (1993) 643;
- [17] M.F.L. Golterman, D.N. Petcher and J. Smit, *Nucl. Phys.* B370 (1992) 51;
W. Bock, A.K. De and J. Smit, *Nucl. Phys.* B388 (1992) 243;
M.F.L. Golterman, D.N. Petcher and E. Rivas, *Nucl. Phys.* B377 (1992) 405; *Nucl. Phys.* B395 (1993) 596;
W. Bock, E. Focht, A.K. De and J. Smit, *Nucl. Phys.* B401 (1993) 481; *Nucl. Phys. B (Proc. Suppl.)* 30 (1993) 666;
S. Aoki, H. Hirose and Y. Kikukawa, preprint UTHEP-256.
- [18] W. Bock, A.K. De, K. Jansen, J. Jersák, T. Neuhaus and J. Smit, *Nucl. Phys.* B344 (1990) 207.

- [19] N. Kawamoto and J. Smit, Nucl. Phys. B192 (1981) 100.
- [20] A. Hasenfratz, K. Jansen, J. Jersák, C.B. Lang, T. Neuhaus and H. Yoneyama, Nucl. Phys. B317 (1989) 81.
- [21] M. Göckeler and G. Schierholz, Nucl. Phys. B (Proc. Suppl.) 29B,C (1992) 114; Nucl. Phys. B (Proc. Suppl.) 30 (1993) 609.

Figure 1: *The κ - y phase diagram of the ISF model. The solid lines represent the phase transitions between the various phases. All phase transitions appear to be of second order.*

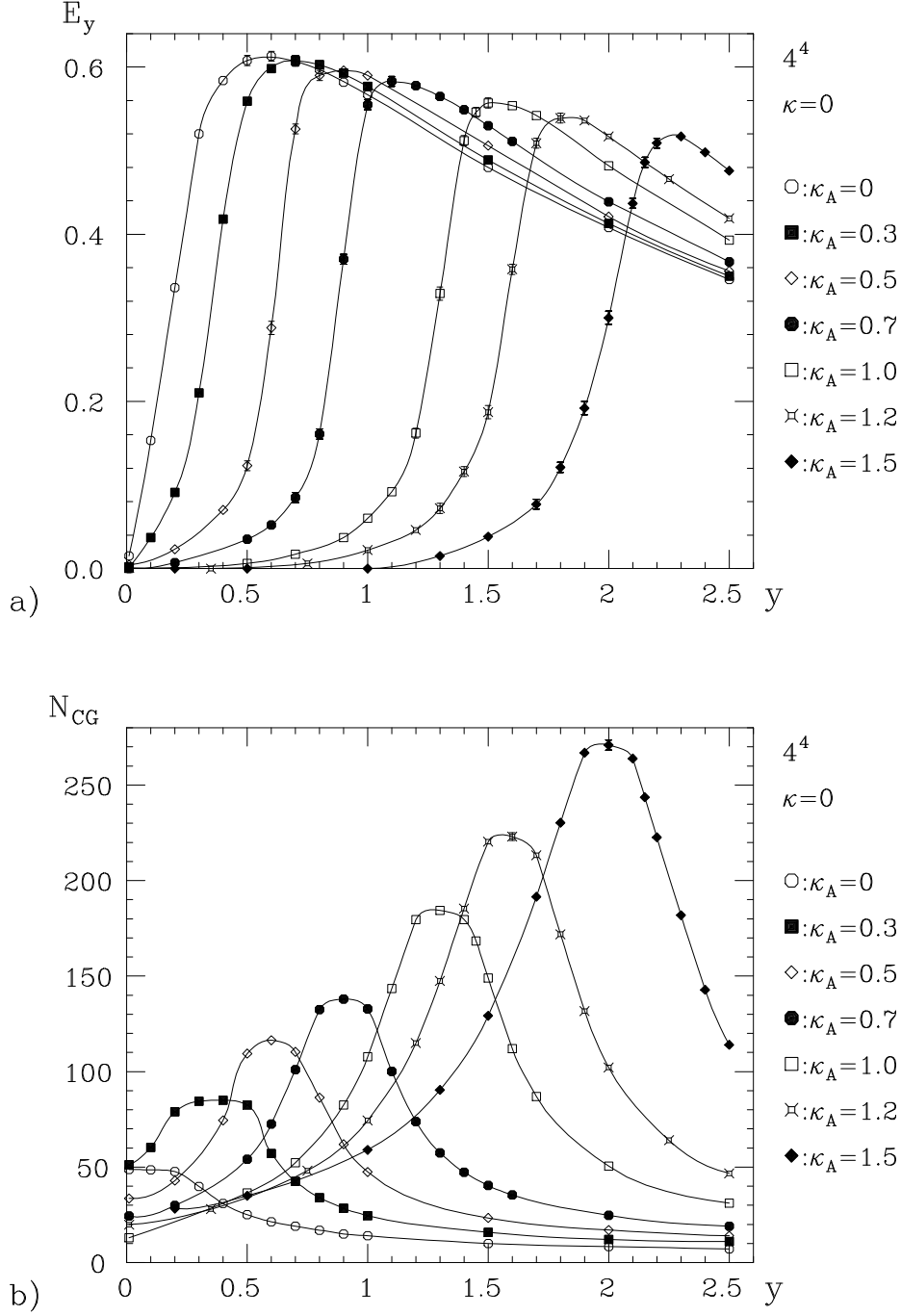


Figure 2: a) The energy E_y as a function of y for several values of κ_A and $\kappa = 0$ in the ISF model. b) The quantity N_{CG} for the same set of bare coupling parameters. Here and in the following we omit the error bars whenever they are smaller than the symbol size.

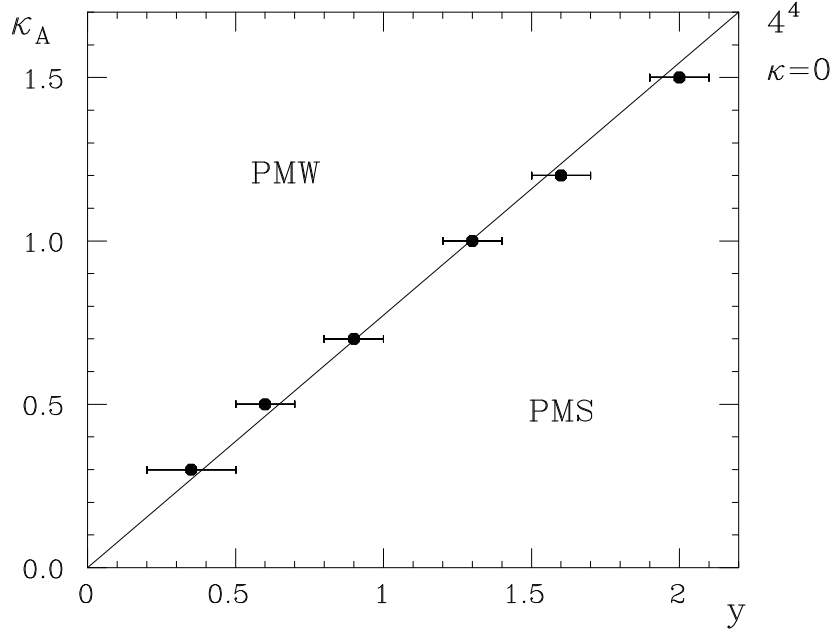


Figure 3: The phase diagram of the IFS model in the κ_A - y plane for $\kappa = 0$. The lattice size is 4^4 .

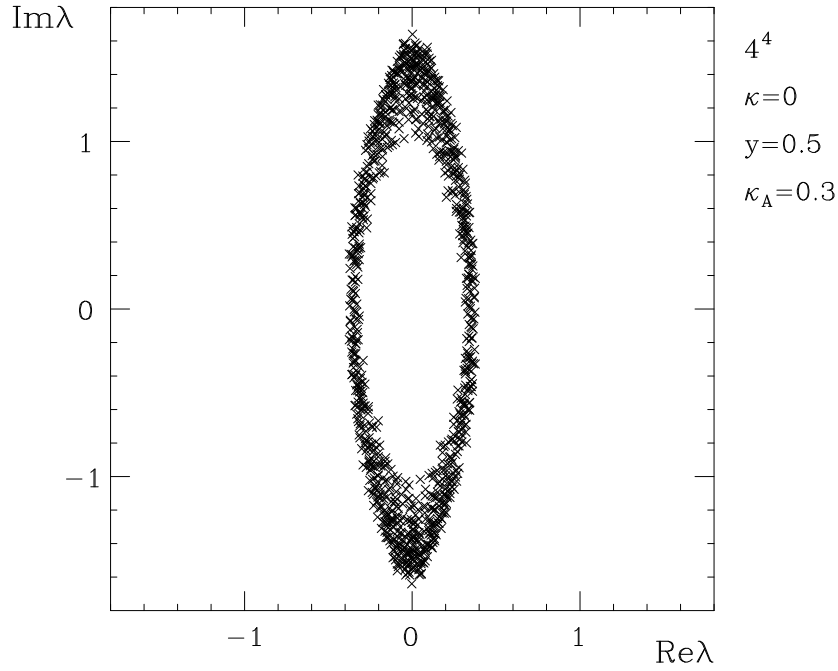


Figure 4: The eigenvalues of the matrix $M_{ISF}^{off} = M_{ISF} - y\mathbb{1}$ plotted into the complex plane. The graph contains the eigenvalue spectra for four independent scalar field configurations which were generated with the HMCA at $(\kappa, y, \kappa_A) = (0, 0.5, 0.3)$. The lattice size is 4^4 .

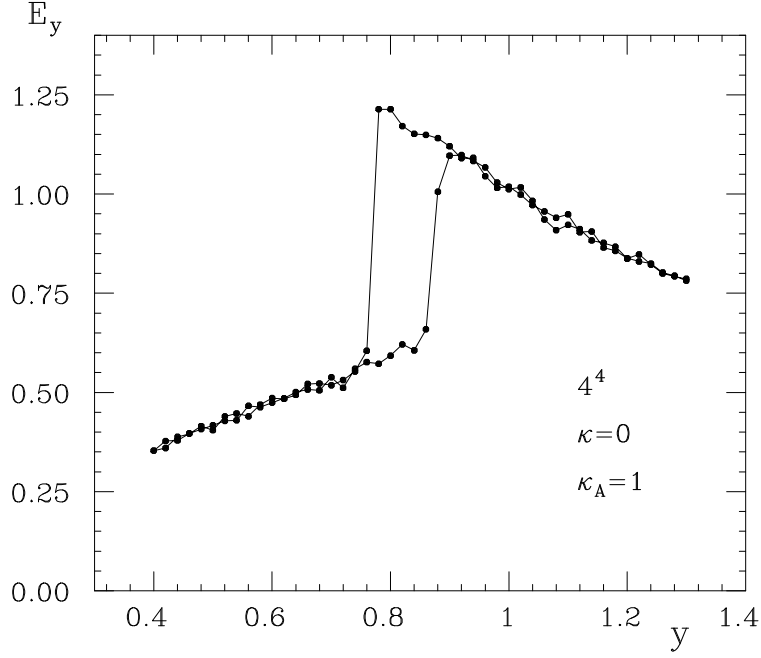


Figure 5: The energy E_y as function of y for $\kappa = 0$ and $\kappa_A = 1$ in the NISF model. The points were obtained in a thermal cycle starting at $y = 1.3$ with a step size of $\Delta y = 0.02$. Each point was obtained by taking the average over 50 HMCA trajectories.

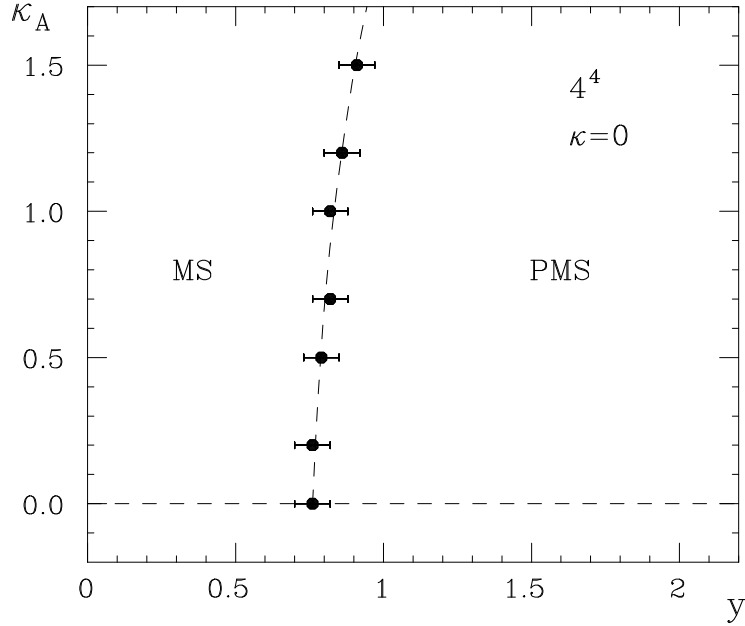


Figure 6: Phase diagram of the NISF model in the κ_A - y plane obtained for $\kappa = 0$. The dashed line indicates that the phase transition between the multi-state (MS) region and the PMS phase is of first order.

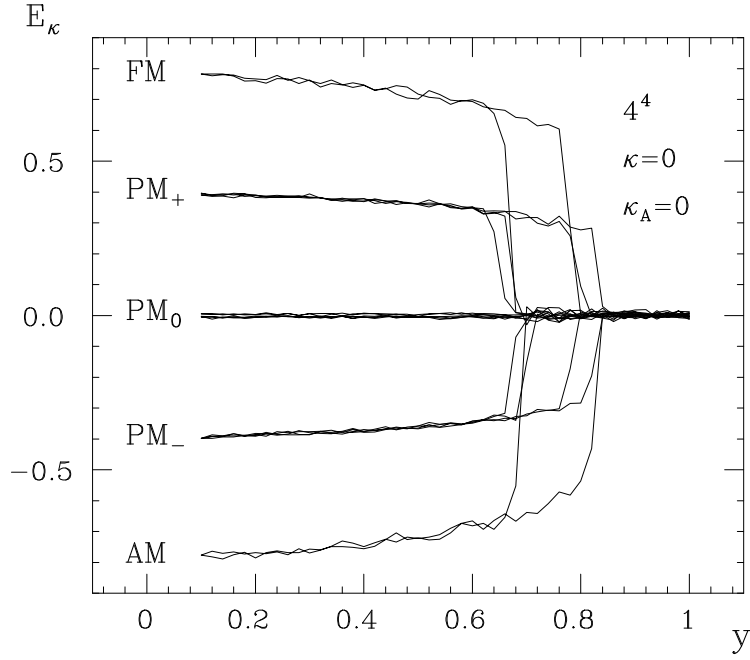


Figure 7: The energy E_κ as a function of y for $\kappa = 0$ and $\kappa_A = 0$ in the NISF model. The plot contains nine thermal cycles, which were started at $y = 1$ inside the PMS phase with a step size $\Delta y = 0.02$. The plot shows that the system can tunnel into five different states when lowering y across the MS-PMS phase transition. Each point in a thermal cycle results from averaging over 50 HMCA trajectories.

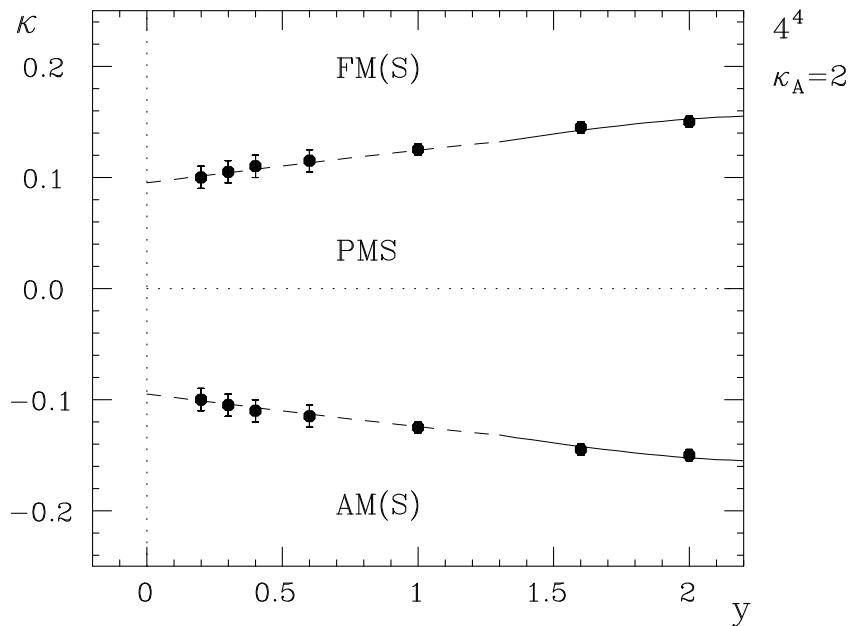


Figure 8: The κ - y phase diagram of the modified NISF model for $\kappa_A = 2$. The solid lines represent the phase transitions of second and the dashed lines phase transitions of first order.

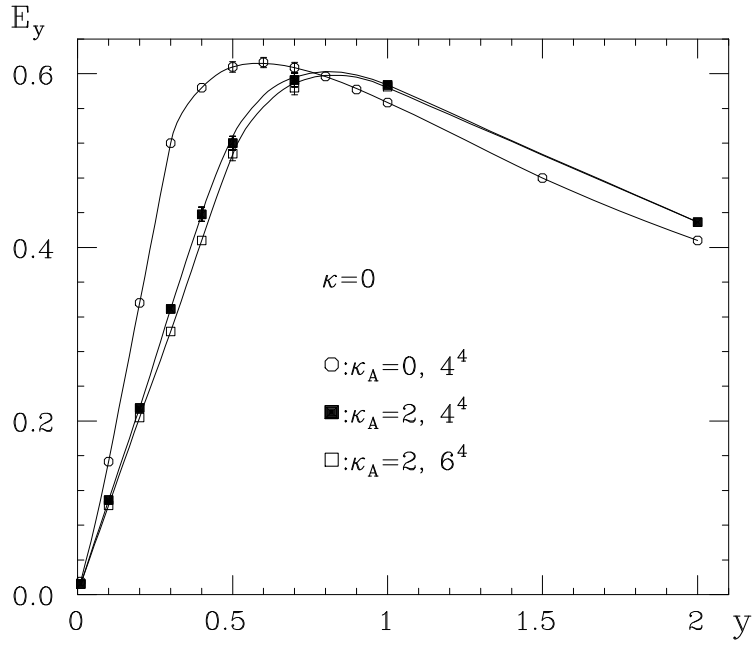


Figure 9: The energy E_y as a function of y in the modified NISF model for $\kappa = 0$ and $\kappa_A = 0, 2$.

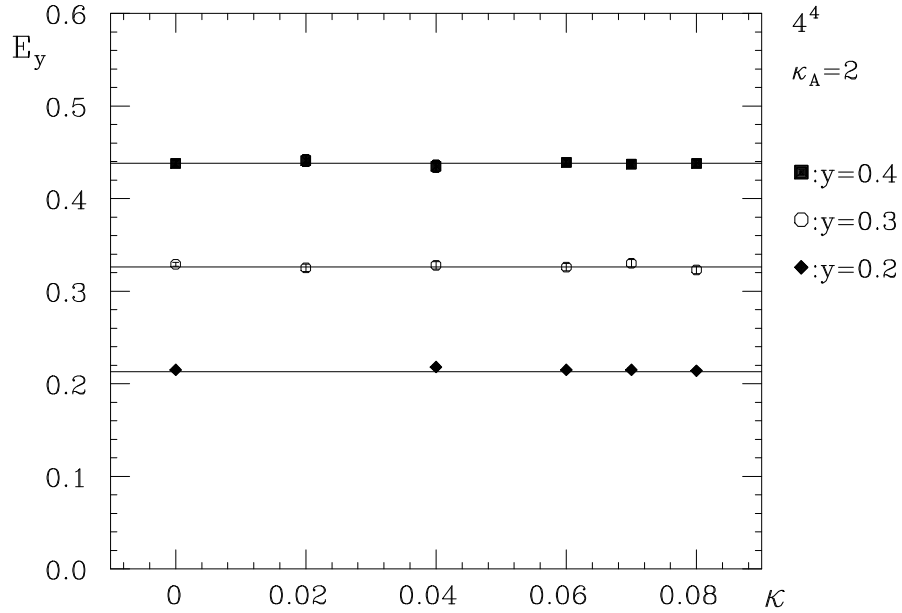


Figure 10: The energy E_y as a function of κ for three values of y and $\kappa_A = 2$ in the modified NISF model.

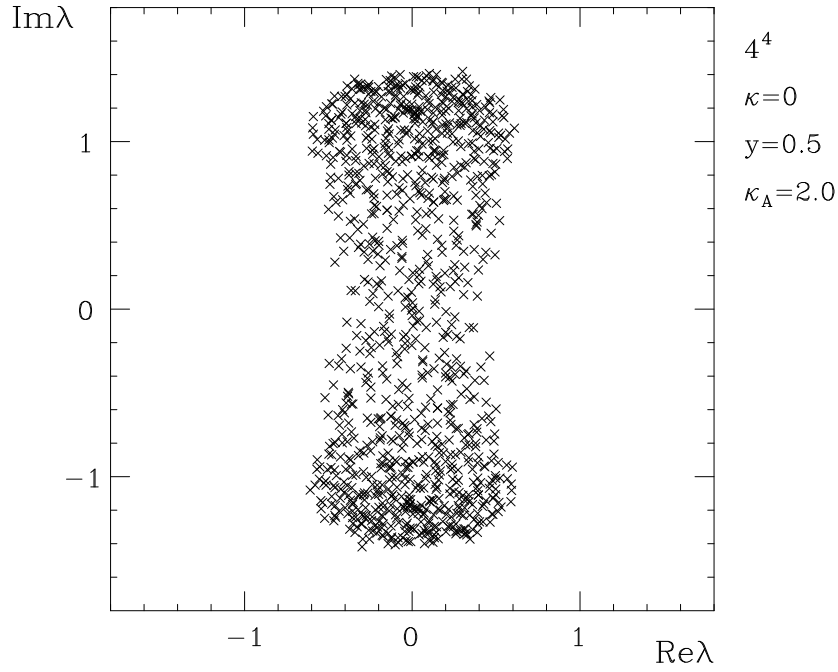


Figure 11: The eigenvalues of the matrix $M_{NISF}^{off} = M_{NISF} - y\mathbb{I}$ plotted into the complex plane. The plot contains the eigenvalue spectra for four independent scalar field configurations which were generated with the HMCA at $(\kappa, y, \kappa_A) = (0, 0.5, 2)$. The lattice size is 4^4 .

